

# Fully Relativistic Quark Models for Heavy-Light Systems

S. A. Pernice

Department of Physics and Astronomy

University of Rochester, Rochester, NY, 14627-0171

September 9, 2018

e-mail: [sergio@charm.pas.rochester.edu](mailto:sergio@charm.pas.rochester.edu)

## Abstract

A fully relativistic quark model is constructed and applied to the study of wave-functions as well as the spectrum of heavy-light mesons. The free parameters of the model are a constituent quark mass and (on the lattice) an adjustable  $r$ -parameter in the fermionic kinetic energy, while the confinement is introduced via potentials measured by MonteCarlo. The results are compared to Monte Carlo energies and Coulomb-gauge wave functions. They are in very good agreement with the data. A comparison with previous models suggests that we are seeing in the Monte Carlo data the quantum-relativistic delocalization of the quark due to Zitterbewegung.

# 1 Introduction

Recent studies in quenched lattice QCD [1] have led to a considerable advance in our understanding of meson wave functions - in particular, of the relation between the Bethe-Salpeter wavefunction of a heavy-light meson in Coulomb gauge QCD and the wavefunctions obtained from a spinless relativistic quark model (SRQM) defined by a Hamiltonian of the form [2, 3]

$$H_1 = \sqrt{p^2 + m^2} + V(r) \quad (1)$$

where  $m$  is a constituent quark mass, and  $V(r)$  the confining potential (determined by Monte Carlo measurements of Wilson line correlations of static color sources).

Wave functions obtained from (1) have proved to be enormously useful in constructing appropriately smeared lattice operators for heavy-light mesons [1], leading to accurate lattice calculations of B-meson properties. They have also been recently applied to the extraction of the Isgur-Wise function [4]. Relativistic potential models have also been used to estimate pseudoscalar meson decay constants [5]

Despite the fact that SRQM wavefunctions give a vastly better fit than nonrelativistic ones to the meson wavefunctions measured in Monte Carlo calculations, some persistent discrepancies in simultaneously describing the asymptotic (large distance) behavior as well as the wavefunction at the origin suggest that the model defined by Eq(1) is not capturing all of the essential physics, even at the level of a valence quark description. Recall that the SRQM of (1) has only a single free parameter, the constituent quark mass  $m$ , as the potential  $V(r)$  is determined by Monte Carlo measurements for each lattice studied. These discrepancies are not very important in constructing

smear operators for the ground state meson in each angular momentum channel, but become very troublesome when one tries to extract excited state properties using the multistate formalism of Ref[1], where admixtures of the ground state should be kept to a minimum.

Our objective in this paper is not only to construct an improved version of the SRQM which does a better job in fitting the global behavior of meson wavefunctions for different angular momenta and for small as well as large distance, but also to provide a clear explanation of the approximations being done and the relation of the resulting model with a hypothetical full QCD solution of the problem.

The resulting model extracts, we believe, the full content of the physical picture provided by the valence quark description and consistent with QCD. The accurate predictions for the wave functions as compared to Monte Carlo simulations (see Section 3.1) indicates that Heavy-light mesons can be represented reasonably well in terms of this picture.

The two main effects which emerge from the more complete treatment given in Sections 2 and 3 below of the lattice QCD Coulomb gauge Hamiltonian, and which are found to improve considerably the agreement of the model with the measured Monte Carlo wavefunctions are

1. A renormalization of the Wilson  $r$ -parameter away from the bare value ( $r=1$ ) used in the Monte Carlo simulations. The sign of this lattice effect can be understood already from the one-loop seagull correction (see Section 2.1), although the magnitude (as in the case of the quark mass correction renormalizing  $K_c$ ) seems to involve a large nonperturbative piece. This is reasonable, since a renormalization of  $r$  is an effect involving *all* momenta, in particular low momenta where we know

perturbation theory fails. Also, one must keep in mind that a one-loop calculation in the 4-dimensional Euclidean theory (with  $a_t \neq 0$ ), will not necessarily give the correct quantitative shift of the spatial  $r$ -parameter in the Hamiltonian formulation (where a continuum limit  $a_t \rightarrow 0$  has implicitly been taken).

This effect, which should become irrelevant in the continuum limit, plays however an important quantitative role improving the agreement between model and data for the lattice sizes tested so far (see section 2.2).

2. Some of the observed discrepancies between model  $H_1$  and the Monte Carlo simulations persist, even after the corrections implied in point 1. These remaining discrepancies are considerably reduced when the correct relativistic treatment of the heavy-light system is performed. A detailed analysis of the differences between this correct treatment and the previous models give rise to a beautiful explanation of this new corrections. They turn out to be due to the delocalization of the light quark known as Zitterbewegung, that, as is well known, arise from the inability to localize a relativistic particle in a local unitary theory. To my knowledge, these effects are seen for the first time in Monte Carlo measured wave functions.

In section 2, we construct a model that correctly takes into account the Wilson lattice fermionic kinetic energy [6] used in the Monte Carlo simulations. This model however does not represent an improvement over  $H_1$ . The reason for that is analyzed and as a result a new model arises, incorporating the renormalization of the Wilson  $r$ -parameter, that does represent

an improvement over (1). In section 2.2 we compare this new model and  $H_1$  with the Monte Carlo data. In section 3 we carry out a fully relativistic treatment of the problem. In section 3.1 this model is compared with the Monte Carlo data. In section 4 we compare the physical content of the three models and interpret the differences. In section 5 we present the conclusions and discuss upcoming studies.

## 2 Improved Treatment of Kinetic Terms

As was shown in Refs. [1, 2], the Hamiltonian given by equation (1) describes very well the results of Monte Carlo calculations of the Coulomb gauge wave functions of a heavy-light meson in quenched approximation. In addition to practical implications for lattice studies, this model provides a surprisingly simple physical picture for the heavy-light mesons, namely, the heavy quark acting as a source of the confining Coulomb potential and the light quark moving relativistically in this confining field (the relativistic nature of the kinetic energy was essential [2] in reproducing the large distance behavior of the wave function). The real gluons are completely decoupled from the quarks except for their role renormalizing the mass.

In this paper, we will carry the physical picture implied by a valence quark model to its limits. The resulting model highly improves the one given by Eq.(1) both conceptually and in its predictive power while keeping the underlying simplicity.

## 2.1 Using the Wilson Action

A first, perhaps obvious modification to  $H_1$  amounts to replacing the kinetic energy by the lattice Wilson dispersion relation [6] taking correctly into account the specific lattice formulation employed in the simulations. It is important in assessing the quantitative validity of the relativistic quark model that systematic effects due to lattice discretization be dealt with consistently both in the model and in the Monte Carlo simulations so that deviations between the two may be properly attributed to important physical effects rather than lattice artifacts which will eventually disappear in the continuum limit. The Monte Carlo calculations [1] that constitute the ‘experimental’ data were done with a Wilson  $r$  parameter equal to one. So our new Hamiltonian becomes:

$$H' = \sqrt{M^2(\mathbf{q}) + \sum_{i=1}^3 \mathbf{Q}_i^2} + V(r) \quad (2)$$

where

$$M(\mathbf{q}) \equiv m + \sum_{k=1}^3 (1 - \cos q_k) \quad (3)$$

$$\mathbf{Q}_k(\mathbf{q}) \equiv \sin q_k \quad (4)$$

Although this model is closer to lattice QCD since it contains the correct dispersion relation, the corresponding wave functions *do not* represent an improvement with respect to model (1). Actually, they magnify the discrepancies between model  $H_1$  and Monte Carlo data. This is at first sight very surprising because, as already said, Eq(2) is closer to lattice QCD in its treatment of the fermionic kinematics than  $H_1$ .

The solution to this puzzle comes from a detailed analysis of the renormalization of the parameters of the theory *on the lattice*.

More specifically, consider the one loop contribution to the quark self energy. On the lattice we have *two* graphs rather than one (as a consequence of the compact representation of the gauge field):

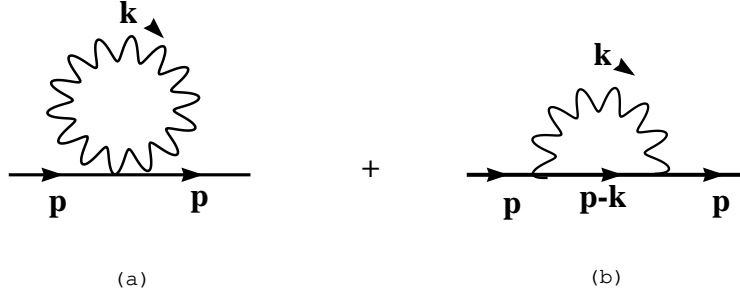


Figure 1: One loop graphs contributing to the quark self-energy

Corresponding to:

$$\tilde{\Gamma}_p \equiv \tilde{\Delta}_p^{-1} - \Sigma_p = m + \frac{r}{2}\hat{p}^2 + i\gamma \cdot \bar{p} + \Sigma_p^{(a)} + \Sigma_p^{(b)} \quad (5)$$

where  $\hat{p} = 2 \sin \frac{p_\mu}{2}$  and  $\bar{p}_\mu = \sin p_\mu$ .<sup>1</sup>

Graph (b) also appears in the continuum while graph (a) is present only on the lattice in a compact formulation of the gauge theory. It is precisely graph (a) that will provide in the cleanest way the solution to our puzzle, as its contribution to the self energy in Coulomb gauge is:

$$\Sigma_p^{(a)} = g^2 \frac{(N^2 - 1)}{4N} \left[ \frac{1}{\Omega} \sum_k \frac{1}{\hat{k}_i^2} \right] (r \cos p_0 - i\gamma_0 \bar{p}_0) + \quad (6)$$

$$g^2 \frac{(N^2 - 1)}{4N} \sum_{i=1}^3 \left[ \frac{1}{\Omega} \sum_k \frac{1}{\hat{k}_\mu^2} \left( 1 - \frac{\hat{k}_i^2}{|\hat{k}_j^2|} \right) \right] (r \cos p_i - i\gamma_i \bar{p}_i) \quad (7)$$

where  $\Omega = L^4$ , greek indices run from 1 to 4 and roman indices from 1 to 3 (this convention applies in all equations in this paper) . Eq(6)contains

<sup>1</sup>We are using here the notation of Ref[7]

the contribution from the Coulombic instantaneous interaction while Eq(7) contains the contributions from the real gluons.

Writing  $\hat{p}^2$  as  $\sum_{\mu=1}^4 2(1 - \cos p_\mu)$ , the inverse free propagator becomes

$$\tilde{\Delta}_p^{-1} = m + 4r - r \sum_{\mu=1}^4 \cos p_\mu + i\gamma \cdot \bar{p} \quad (8)$$

and we immediately realize that the part of  $\Sigma_p^{(a)}$  proportional to the identity matrix (in the Dirac indices) explicitly renormalizes the Wilson  $r$  parameter. Specifically:

$$r_{\text{time}} \rightarrow r \left\{ 1 - g^2 \frac{(N^2 - 1)}{4N} \left[ \frac{1}{\Omega} \sum_k \frac{1}{\hat{k}_i^2} \right] \right\} \quad (9)$$

$$r_{\text{space}} \rightarrow r \left\{ 1 - g^2 \frac{(N^2 - 1)}{4N} \left[ \frac{1}{\Omega} \sum_k \frac{1}{\hat{k}_\mu^2} \left( 1 - \frac{\hat{k}_i^2}{|\hat{k}_j^2|} \right) \right] \right\} \quad (10)$$

For our lattice size, the perturbative  $r$  renormalization due to graph (a) are, in Coulomb gauge:

$$\delta r_{\text{time}}^{V=12^3} = -g^2 \frac{(N^2 - 1)}{4N} 0.234 = -0.452 \quad (11)$$

$$\delta r_{\text{space}}^{V=12^3} = -g^2 \frac{(N^2 - 1)}{4N} 0.102 = -0.197 \quad (12)$$

We shall be comparing RQM models with MonteCarlo data generated on a  $12^3 \times 24$  lattice at  $\beta = 5.7$ , corresponding to a naive bare lattice coupling  $g_0^2 \sim 1.05$ . The hopping parameter was  $\kappa = 0.168$ . Nonperturbative effects may partially be included by using instead the tadpole-improved [10] definition of the coupling, which gives for the  $\beta$  value considered a value closer to 2.9 for  $g^2$  [2]. This is the value used in Eqs(11,12).

In our Hamiltonian models we consider of course only  $r_{\text{space}}$ . This value, as we will see in the next subsection correctly predict the sign of the change in



$r$  although the magnitude seems to have big nonperturbative contributions. Graph (b) also contributes *effectively* to the  $r$  renormalization, but not in an explicit way as in the case of the first one. However, in this case the numerical contribution is much smaller (as in the case of the mass shift).

Of course the mass is also renormalized as is well known, and also by an amount which is quite a bit larger than the perturbative one-loop shift (even with tadpole improved couplings).

The important point of this calculation is to realize that *not only the mass but also the Wilson  $r$  parameter should be considered as free parameters, since both of them are dynamically modified, in a nonperturbative way.*

Including this effect, the model acquires the same form as in Eq(2)

$$H_2 = \sqrt{M^2(\mathbf{q}) + \sum_{i=1}^3 \mathbf{Q}_i^2} + V(r) \quad (13)$$

but with

$$M(\mathbf{q}) \equiv m + r \sum_{k=1}^3 (1 - \cos q_k) \quad (14)$$

We have now therefore *two* adjustable parameters,  $m$  and  $r$ . This new model, with correctly chosen values for the parameters, represents a substantial quantitative improvement over model (1) as will be shown in the next section. We also understand now why Eq.(2) actually works worse than Eq(1), as  $H_1$  is *effectively* close (in the sense that the fermionic kinetic dispersion relation is close to the bosonic one over most lattice momenta) to one particular case of the model  $H_2$ . In fact, it corresponds, for fixed  $m$ , to  $r \approx 0.85$  as can be seen simply by plotting the corresponding dispersion relations. This value, although not optimal, is closer to the optimal choice for model (13) (see Section 2.2) than the naive unrenormalized choice  $r = 1$ .

The improvement obtained with Eq (13), although very significant from a quantitative point of view for the lattice sizes tested so far , should nevertheless become irrelevant in the continuum limit, although it is certainly relevant in providing accurately smeared meson operators for multistate MonteCarlo studies [1].

In any case, we have now not only a better model but one that has a closer connection to QCD since it contains the actual *dynamical* QCD fermionic kinetic energy . We shall see in the next section that the modification in the dispersion formula greatly improves the fit to the measured wavefunctions at shorter distance (and in particular at the origin) once the  $m$  and  $r$  parameters are chosen to optimize the fit at medium and large distances.

A fuller description, starting with the Bethe-Salpeter equation (which for a light quark propagating in the color field of a static source reduces to a Dirac equation) will lead in Section (3) to a model giving similar wavefunctions, agreeing even more closely with the measured ones. Such a model represents a valence quark description of the heavy-light meson that is as close to QCD as possible without leaving the physical picture outlined in the introduction.

## 2.2 Quantitative Consequences of the Improved Potential Model

In order to actually solve for the wave functions of the model, we used the same method as in Refs [1, 2]. We briefly explain it here for completeness.

The procedure used in a multistate smearing calculation of heavy-light meson properties [2] for generating lattice smearing functions from the RQM

is as follows. One obtains orthonormal lattice wavefunctions, which are eigenstates of a lattice RQM Hamiltonian defined on a  $L^3$  lattice (with  $\vec{r}, \vec{r}'$  lattice sites):

$$H_{\vec{r}\vec{r}'} \equiv K_{\vec{r}\vec{r}'} + V(\vec{r})\delta_{\vec{r}\vec{r}'} \quad (15)$$

The eigenstates in a channel of given orbital quantum numbers (S,P,D etc) are obtained by applying the resolvent operator  $\frac{1}{E-H}$  to a source wavefunctions of the same orbital symmetry. The model at this stage is spinless (the measured wavefunctions represent spin-averages of the top two Dirac components of the light quark field) so issues of spin-orbit coupling do not yet arise (they will be dealt with properly in the full Dirac formalism of Section 3).

In the resolvent approach, S-states are generated by applying the resolvent kernel to a monopole localized at the origin, P-states with a source dipole, and so on. At each trial value of the energy  $E$ , the norm of the resulting state  $\frac{1}{E-H}\Psi^{(0)}$  is evaluated. Obviously

$$R \equiv \left\| \sum_{\vec{r}'} \left( \frac{1}{E-H} \right)_{\vec{r}\vec{r}'} \Psi^{(0)}(\vec{r}') \right\| \rightarrow \infty \quad (16)$$

when  $E \rightarrow$  eigenvalue of  $H$ . Typically, wavefunctions accurate to 4-5 significant figures are obtained by stopping once this norm exceeds 3000. At this point a smearing eigenstate  $\Psi_{\text{smear}}^{(a)}(\vec{r})$  is extracted by renormalizing the vector  $\frac{1}{E-H}\Psi^{(0)}$  to unit norm. The inversion of  $E-H$  is performed by the conjugate gradient algorithm, with the multiplication of the kinetic term done in momentum space using a fast Fourier transform.

In the following figures we present the results of our new model as compared with the old one. As was already mentioned in the previous section,

the MonteCarlo data presented in the following figures was generated on a  $12^3 \times 24$  lattice at  $\beta = 5.7$ , and the hopping parameter was  $\kappa = 0.168$ .

In Fig[2] we compare the ground state wave functions for the  $V = 12^3$  case. The values chosen for the constituent mass and  $r$  parameters are chosen to maximize the agreement (in a mean square sense) between data and the respective models *in the ground state*. As it turned out, the optimum constituent masses are very similar to one another and the wave functions very insensitive to small changes around the optimum value. We present here the results for the same values of the constituent mass. This choice, while essentially identical to the optimum cases, helps to appreciate the effect of the  $r$  renormalization. The case of  $H_2$  with  $r = 1$  is also included to emphasize the effect of the  $r$  renormalization. As we can see, the agreement with the Monte Carlo data was already very good for  $H_1$  and is further improved, specially at the origin by  $H_2$ .

But the most important reason for which model  $H_2$  was introduced, was to capture the lattice artifacts unavoidably present in the Monte Carlo data. Only after these artifacts are well under our control can we hope to find some physics in the data beyond the one provided by  $H_1$ . In this sense the improvement at the origin is due to the  $r$  renormalization as can be seen by comparing with the unrenormalized case denoted  $H_2$ ,  $m = 0.23$ ,  $r = 1.0$ . Also we present in Fig[3] a detail of Fig[2] corresponding to the region of distances between  $R = 1.4$  and  $R = 2.4$ . Specifically, as can be seen in Fig[2], at points corresponding to distances  $R_1 = \sqrt{3}$  ( this corresponds to the lattice points  $\vec{x}_1 = \pm 1\hat{i} \pm 1\hat{j} \pm 1\hat{k}$  ) and  $R_2 = 2$  (corresponding to the point  $\vec{x}_2 = \pm 2\hat{i} \pm 0\hat{j} \pm 0\hat{k}$  and the points generated by cyclic permutation of the coordinates), there is a pronounced ‘discontinuity’ in the Monte Carlo

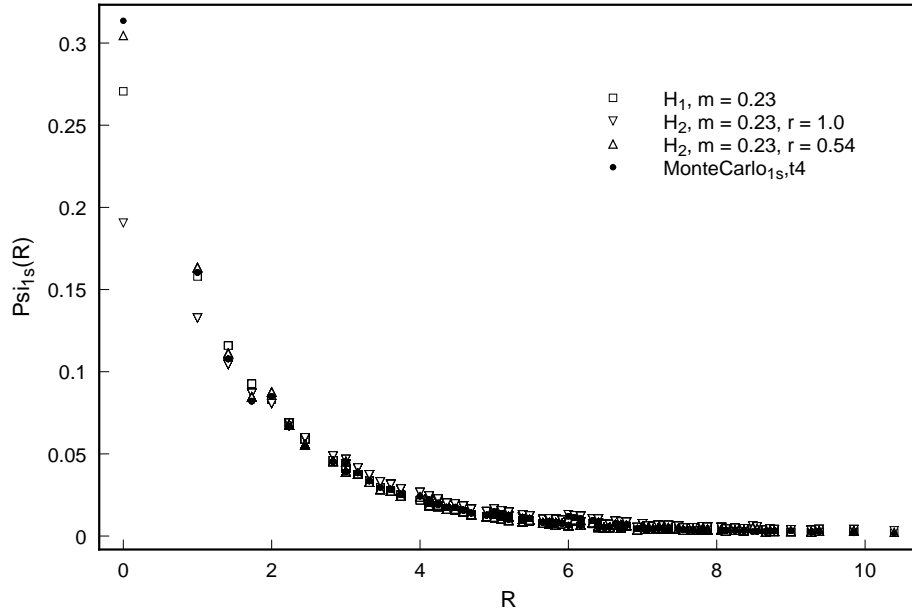


Figure 2: 1S state,  $L = 12$ . We see at the origin the improvement of  $H_2$  over  $H_1$  when  $r$  is renormalized. With  $r = 1$  however, model  $H_2$  does a poor job showing the necessity of  $r$  renormalization. The Monte Carlo wave functions were extracted at different time slices. Although all time slices gave very similar results, the wave function extracted at the fourth one, that we present here, was the one with the best signal to noise ratio. That is the meaning of the t4 in the Monte Carlo data point label.

data that should of course disappear in the continuum limit. On a finite lattice and still not very close to the continuum this discontinuity is easy to understand qualitatively: it is due to the fact that under these conditions the system responds more naturally in terms of a metric notion of distance between two points on a lattice given by some function of the number of links between these points (notice that  $\vec{x}_1$  is at 3 links away from the origin while  $\vec{x}_2$  is only at 2, in contradistinction with their euclidean distance). In figure 3 we see how model  $H_1$  completely ignores this lattice artifact,  $H_2$  with  $r = 1$  is slightly closer, while  $H_2$  with  $r = 0.54$  follows almost perfectly the discontinuity.

In Fig[4] we can better appreciate the large distance region.

In Fig[5], we show the same information as in Fig[2] but in logarithmic scale to appreciate the asymptotic region. As we see, both,  $H_1$  and  $H_2$  with renormalized  $r$  do a very good job in this region.

So, as we have seen, as far as the ground state is concerned,  $H_2$  not only shows an improvement over  $H_1$  specially visible at the origin, but it also proved capable of capturing very pronounced lattice artifacts. Both effects clearly show the relevance of taking into account the  $r$  renormalization.

Once the values of  $m$  and  $r$  are specified to reproduce as accurately as possible the ground state, we compare now the results for the 1P state. In this case, we divide the respective wave functions by  $\cos\theta$  to show only the radial dependence. As we can see in Fig[6], the model  $H_2$  does again a better job than  $H_1$ , although there is still room to improve. The case of  $H_2$  with  $r = 1$  is not shown since it was in the previous figures only to see the effect of renormalizing  $r$ . In any case, it again performs worse than  $H_1$ .

So we conclude that, although the modifications leading to  $H_2$  are only

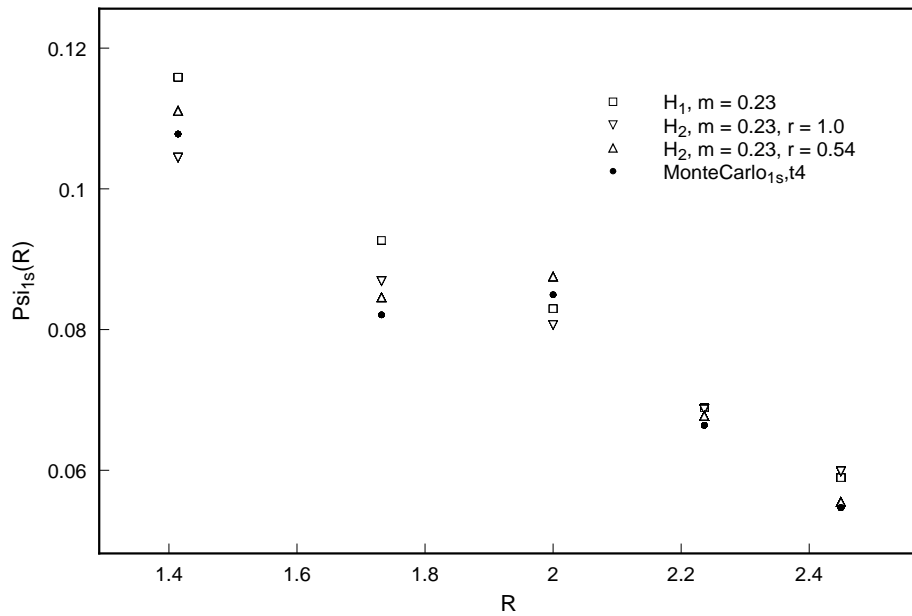


Figure 3: Detail of figure 2. We see here the ‘discontinuity’ between points at distances  $R_1 = 1.73$  and  $R_2 = 2$ . While model  $H_1$  completely ignores it, and model  $H_2$  with unrenormalized  $r$  can do just slightly better, model  $H_2$  with the renormalized  $r$  almost perfectly follows the discontinuity.

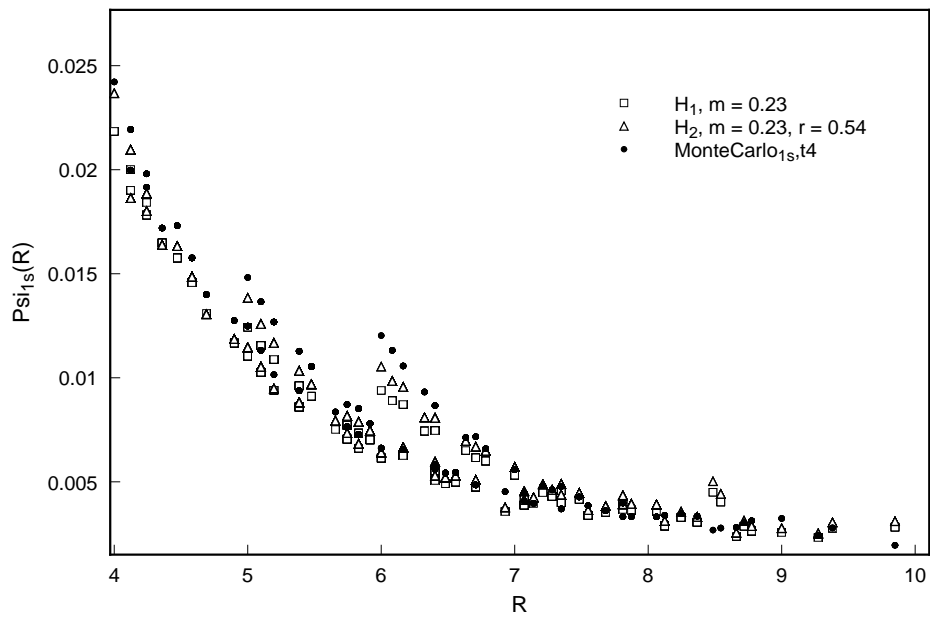


Figure 4: Large  $R$  region of figure 2. The case  $H_2$  with  $r = 1.0$  is not displayed to clarify the relevant information. We see that both  $H_1$  and  $H_2$  with renormalized  $r$  fall very close to the data in this region (notice the scale).



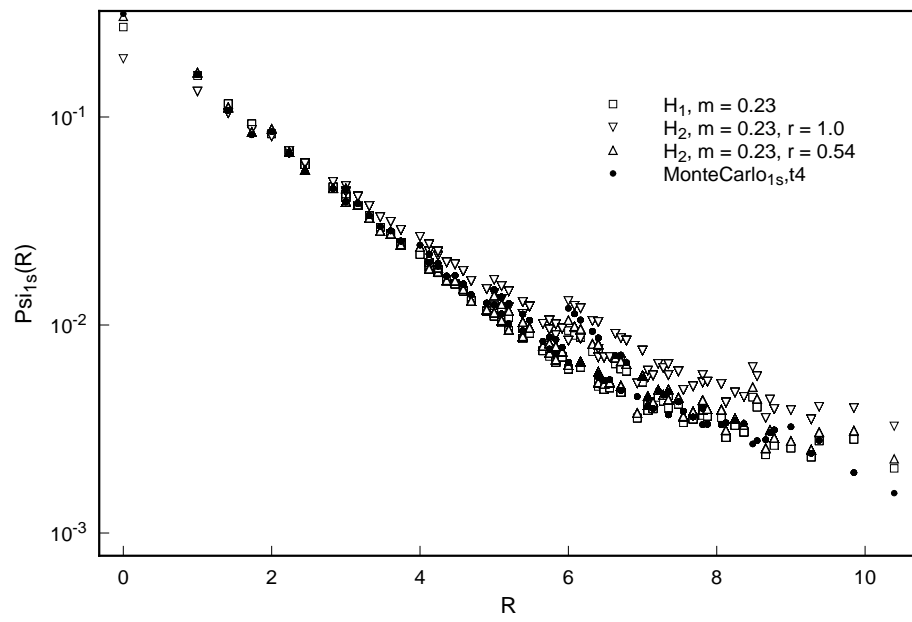


Figure 5: 1S state  $L = 12$ , logarithmic scale. Both,  $H_1$  and  $H_2$  with renormalized  $r$  do a very good job at large distance.

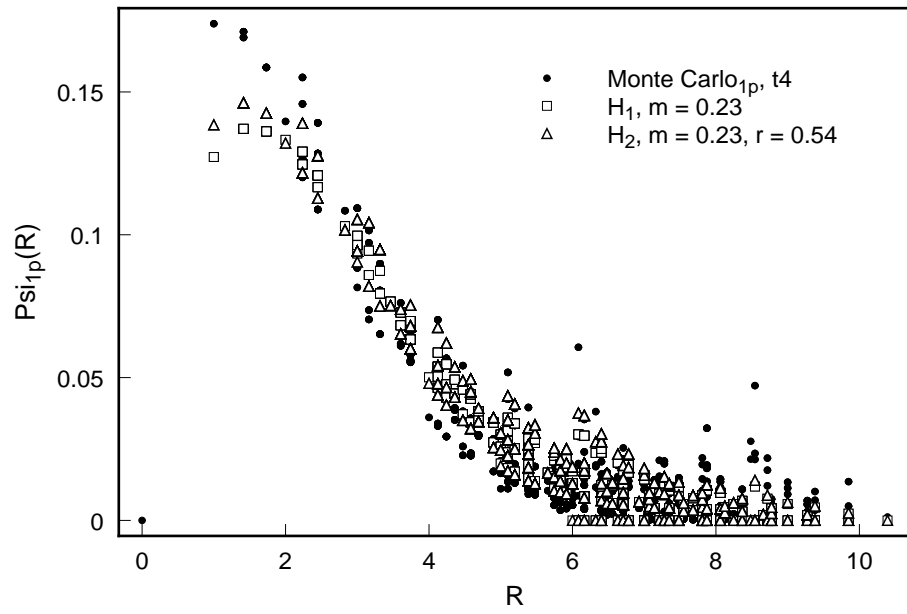


Figure 6: 1P state ,  $L = 12$ . The values of the parameters were fixed to reproduce as accurately as possible the ground state. We can see the improvement of  $H_2$  over  $H_1$ , but still we have plenty of room to improve.

due to lattice artifacts, the quantitative improvement is significant, so the value of  $H_2$  resides in the fact that it captures a very important lattice discretization effect. Nevertheless the improved model is still conceptually and quantitatively inadequate. The conceptual inadequacy stems from the fact that the relation between the eigenstates of  $H_2$  and the spin-averaged Bethe-Salpeter wavefunctions in Coulomb gauge is unclear (e.g. the potential model ignores antiquarks whereas there are coupled upper and lower components in a Dirac formalism). Quantitatively, we shall see that use of a full Dirac formalism which is closely related to the Bethe-Salpeter wavefunction also further improves the agreement with the Monte Carlo results. In this full formalism, it will still be important however to include the  $r$ -renormalization discussed above.

### 3 Full Bethe-Salpeter treatment of Heavy-Light Wavefunctions

As we have seen, the agreement between the wavefunctions derived from the Hamiltonian  $H_2$  and the Monte Carlo data is quite remarkable; however, not only is there still room for further quantitative improvement but from a conceptual point of view the connection between these simple models and a full hypothetical QCD solution of the meson Coulomb gauge wave functions is not completely clear. In another words, it would be nice to have a model that works as well as the previous one and in which the nature of the approximations being done is completely transparent. In this subsection we will construct this model and as a bonus the resulting one will show an additional quantitative improvement over  $H_2$  with a very nice physical

interpretation.

We shall assume that:

- (a) Transverse gluon interactions with the quarks act primarily to renormalize the mass and  $r$  parameters in the quark kinetic term. Fock states involving real gluons in addition to the valence quarks are neglected.
- (b) The net effect of Coulomb gluon exchange between the light and static quarks can be expressed by the potential acting between two infinitely heavy color sources.

More qualitatively, the picture in the back of our mind, supported by the comparison with data as will be seen in Section (3.1), consists of the light quark moving fast enough for relativistic effects to be important, but on the other hand not so fast that the interaction with the static quark cannot be accurately described by the energy which would obtain if the light quark were held fixed. Alternatively, one might assume that the time scales over which the string connecting the quark to the static source responds to changes in the light quark position are small compared with the time scales relevant for the light quark motion.

Before we proceed with the derivation of our new model, it will be useful to present a brief description of what was actually measured in the Monte Carlo simulations of Ref[1] that constitutes our data. Even though this work used a sophisticated multistate smearing method, for our purposes it suffices to know that the basic information was extracted from the measurement, in quenched lattice QCD, of the Green function:

$$F(\vec{x}', \vec{x}, t) = \langle 0 | \bar{Q}_H(\vec{0}, t) \gamma_5 q_H(\vec{x}', t) \bar{q}_H(\vec{x}, 0) \gamma_5 Q_H(\vec{0}, 0) | 0 \rangle \quad (17)$$

in the limit where the b-quark is taken to be infinitely massive. In this

limit, the heavy quark propagator is simply proportional to  $\frac{1-\gamma^0}{2}$ , therefore  $F$  becomes proportional to the average of the upper two components of the light quark propagator in the presence of a color source. From the calculation of this object, using the above mentioned multistate smearing method (i.e. smearing the source point  $\vec{x}$  of the light quark with Ansatz meson wavefunctions derived from  $H_1$ ) the upper two components of the meson wave function were extracted and spin averaged. The result of this operation constitutes the data against which we compare our models.

Taking this into account we will now construct a model that represents as closely as possible the quantities measured in the Monte Carlo simulations realizing at the same time the physical ideas presented above.

In a full QCD treatment of the problem at hand, the relevant Bethe-Salpeter wavefunction would be

$$\chi(\vec{x}, t) \equiv \langle 0 | q_H(\vec{x}, t) \bar{Q}_H(\vec{0}, t) | P \rangle \quad (18)$$

where  $|0\rangle$  is the vacuum,  $|P\rangle$  is the meson state (in the center of mass frame with energy  $H|P\rangle = E_{BS}|P\rangle$ ), and  $q_H, Q_H$  are the light and heavy Heisenberg fields.

In the infinitely massive heavy quark limit, but otherwise still in full QCD, Eq.(18) is best written as,

$$\chi(\vec{x}, t) \equiv \langle 0 | q_H(\vec{x}, t) | P^* \rangle \quad (19)$$

where  $|P^*\rangle \equiv \bar{Q}_H(\vec{0}, t) | P \rangle$ . This notation emphasizes the fact that in the above limit, the heavy quark field is not dynamical.

As we see, if we were able to calculate exactly Eq.(19) in the context of heavy quark limit quenched lattice QCD, we would be reproducing every

detail of the results of the Monte Carlo simulations, since that is precisely the quantity being measured.

In our physical picture however, as stated above the transverse gluon interactions with the quarks act primarily to renormalize the mass (and in the lattice also the Wilson  $r$  parameter) in the quark kinetic term and the net effect of Coulomb gluon exchange between the light and static quarks can be expressed by the potential acting between two infinitely heavy color sources. Under these conditions the equation satisfied by  $q_H$  reduces to:

$$\langle 0 | (\gamma_E^0 \frac{\partial}{\partial t} - i\vec{\gamma} \cdot \vec{\nabla} + i\gamma_E^0 A_0 + m) q_H | P^* \rangle = 0 \quad (20)$$

that together with the Heisenberg equation  $\frac{\partial}{\partial t} q_H = [H, q_H]$  (in Euclidean space) and the relation  $\langle 0 | [H, q_H] | P^* \rangle = -E_{BS} \langle 0 | q_H | P^* \rangle$ , give rise to the eigenvalue equation

$$(-i\vec{\alpha} \cdot \vec{\nabla} + m\beta + V(\vec{r}))\chi(\vec{r}) = E_{BS}\chi(\vec{r}) \quad (21)$$

which is nothing but the Dirac equation for the light quark in the presence of the confining external field. This equation corresponds, on the lattice, (with the renormalization of the Wilson  $r$  parameter also taken into account) to an effective lattice Hamiltonian given by the usual Wilson fermion action:

$$\begin{aligned} H_3 = & \sum_{\mathbf{x}} \{ \chi^+(\mathbf{x})(m + 3r) \beta \chi(\mathbf{x}) \\ & + \frac{i}{2} \sum_{k=1}^3 [\chi^+(\mathbf{x} + \hat{\mathbf{k}}) \alpha_k \chi(\mathbf{x}) - \chi^+(\mathbf{x}) \alpha_k \chi(\mathbf{x} + \hat{\mathbf{k}})] \\ & - \frac{r}{2} \sum_{k=1}^3 [\chi^+(\mathbf{x} + \hat{\mathbf{k}}) \beta \chi(\mathbf{x}) + \chi^+(\mathbf{x}) \beta \chi(\mathbf{x} + \hat{\mathbf{k}})] \\ & + \chi^+(\mathbf{x}) V(\mathbf{x}) \chi(\mathbf{x}) \} \end{aligned} \quad (22)$$

where  $\mathbf{x}$  represents a point in the three dimensional lattice of size  $L$ ,  $\beta$  and  $\alpha_k$  are just the Dirac matrices,  $\chi(\mathbf{x})$  is the 4-component wave function, and

$V(\mathbf{x})$  is the confining potential determined by Monte Carlo measurements of Wilson line correlations of static color sources [1]. The constituent mass  $m$  and the Wilson  $r$  parameters are free parameters.

The Hamiltonian  $H_3$  defines our new model. From the above discussion we realize it represents the closest possible model to QCD consistent with the valence quark picture whose validity in the heavy-light meson system we want to check.

As will be shown in Section (3.1) this new model represents a further improvement in the prediction of the correct wave functions, that by now are, within the errors of the Monte Carlo calculations, essentially fully reproduced, indicating the validity of the valence quark model to describe heavy-light mesons. Given the necessary assumptions to generate this picture from QCD (stated above), the strong coupling nature of the confining mechanisms, and the lightness of one of the quarks clearly reflected in the necessity of a fully relativistic kinetic energy, the success of the model can hardly be expected a priori, and constitutes a strong statement about QCD dynamics.

### 3.1 Comparison with data

To find numerically the eigenvectors and eigenvalues of  $H_3$ , although we followed in general the same procedure outlined in Section(2.2), some features of  $H_3$  had to be taken into account. For example, due to the non-positivity of the spectrum, the inversion of  $E - H_3$  was performed with a generalization of the conjugate gradient algorithm, the so called *minimum residual algorithm* [8], that takes care of symmetric but non-positive definite matrices (one may replace the  $N \times N$  complex hermitian  $H_3$  with a real symmetric

$2N \times 2N$  version, which is however non-positive-definite). To locate the correct region of the spectrum we started in the large mass regime where the wavefunctions are well understood and gradually reduced the mass while tracking the resulting eigenstates.

In the following figures we present the results of our new model and compare them with the Monte Carlo Data and the predictions of  $H_2$ . The values of the parameters are chosen again to reproduce as well as possible the ground state of the system. Following as closely as possible what was done in the Monte carlo simulations, (briefly described in section 3), the results of  $H_3$  presented in the figures, constitute the average of the two upper components of the corresponding four-component eigenvectors.

In Fig[7] we see that our new model performs as well as  $H_2$  for the ground state, where there was essentially no room for further improvement. We should however note that while the optimum value for  $r$  in  $H_3$  suffers only a small change with respect to the one in  $H_2$ , the optimum mass becomes considerably heavier.

Once the parameters have been fixed to reproduce as well as possible the ground state of the system, we may compare the 1P state. Again, as in the previous figures for 1P wave functions, we divide them by  $\cos\theta$  and present only the radial part. In this case we clearly see the quantitative superiority of  $H_3$  over the previous models. Near the origin  $H_3$  falls much closer to the data than  $H_2$ .

We see then that choosing the optimal parameters for the respective models, a full Dirac model based on the operator  $H_3$  (that, as we have seen in section 3 is conceptually as close to lattice QCD as possible within the valence quark model), outperforms all the other models and within Monte



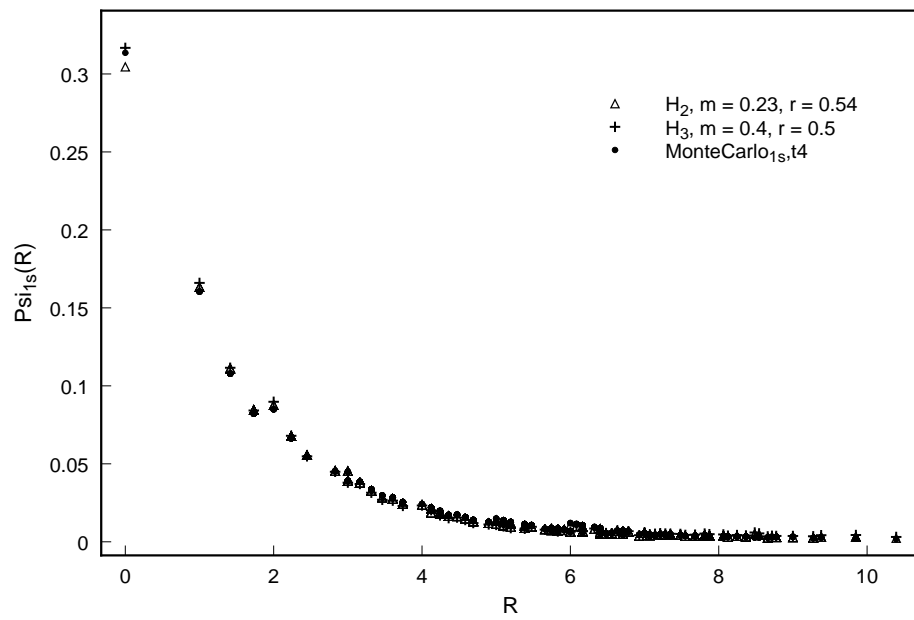


Figure 7: 1S state,  $L = 12$ . The Dirac model performs in this case slightly better than  $H_2$ , although there is little room for further improvement in this case.

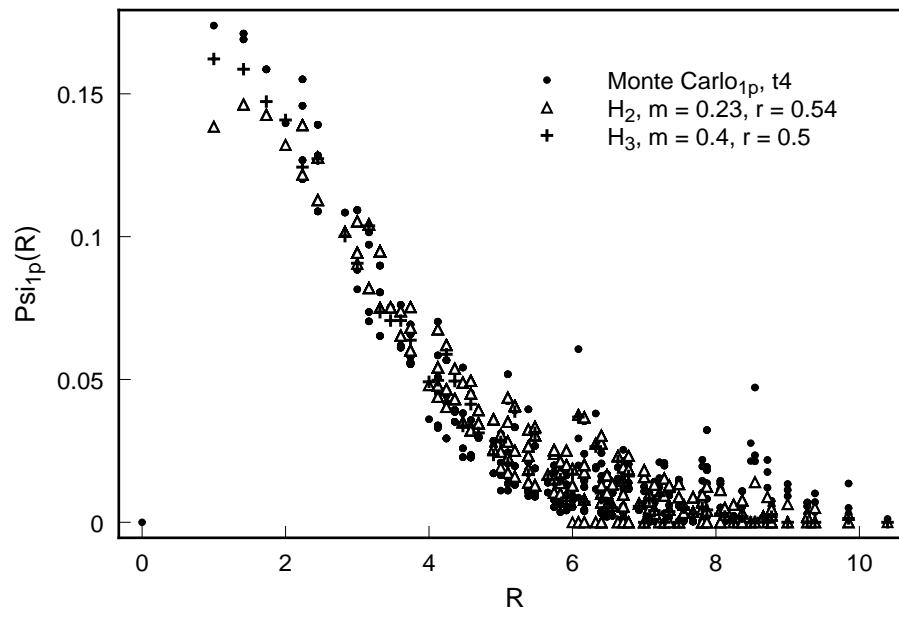


Figure 8: 1P state,  $L = 12$ . The Dirac model performs in this case much better than  $H_2$ .

Table 1:

Model	$E_{2S} - E_{1S}$
Monte Carlo, $\kappa = 0.168$	$0.31 \pm 0.02$
$H_1, m = 0.23$	0.381
$H_2, m = 0.23, r = 0.54$	0.356
$H_3, m = 0.4, r = 0.5$	0.324

Carlo errors essentially fully reproduces the data.

We had also available the energies of the 1S and 2S states for the Monte Carlo data, obtained from the multistate smearing analysis of [1]. The only meaningful comparison is between energy differences since there is an arbitrary choice in deciding the zero energy of the potential  $V(r)$ . The respective energy differences between 1S and 2S states are presented in Table 1.

Again model  $H_3$  is in better agreement with the Monte Carlo results than the others and, within the errors, reproduces the measured results.

Model  $H_3$  was systematically closer to the data for other values of the hopping parameter  $\kappa$ . We present in Table 2 the energy splitting for the Monte Carlo data corresponding to  $\kappa = 0.161$ . This value corresponds to a heavier light quark and the optimum values of the parameters correspondingly change. They are also presented in Table 2. Although the Monte Carlo predictions for the various values of the energies change with respect to the previous ones, the energy difference essentially remains unchanged. This behavior is closely followed by  $H_3$  that continues matching the data. Very interestingly though,  $H_2$  suffers an appreciable modification in the right di-

Table 2:

Model	$E_{2S} - E_{1S}$
Monte Carlo, $\kappa = 0.161$	$0.32 \pm 0.02$
$H_1, m = 0.32$	0.385
$H_2, m = 0.32, r = 0.46$	0.338
$H_3, m = 0.5, r = 0.45$	0.325

rection, it's predictions approach the ones of  $H_3$  for this heavier case. The approach of models 2 and 3 for heavier quarks will be discussed in greater detail in the following section.

In the next section we will discuss the nature of the improvement of  $H_3$  with respect to the previous models.

## 4 Physical Origin of differences

In order to fully appreciate the nature of the quantitative improvement given by our new model, we will now compare it with the previous ones.

An obvious difference between the model given by Eq.(22) and those described by equations (1) and (13) is that the former takes into account spin effects. The Monte Carlo wavefunctions with which we have tested the model were in fact spin-averaged, but  $H_3$  contains in principle a full description of spin-orbit effects. What follows is a comparison of the models at the spin-averaged level. The MonteCarlo wavefunctions obtained in heavy-light simulations are typically obtained by averaging the two upper components of the light quark propagator on the final time slice. That is why we have

performed the same averaging when computing a meson wavefunction from the new RQM.

Expressing the kinetic part of the Hamiltonian  $H_3$  in momentum space, we get,

$$H_{3 \text{ kin}} = \frac{1}{L^3} \sum_{\mathbf{q}} \tilde{\chi}^+(\mathbf{q}) \{ M(\mathbf{q}) \beta + \sum_{k=1}^3 \alpha_{\mathbf{k}} \mathbf{Q}_{\mathbf{k}}(\mathbf{q}) \} \tilde{\chi}(\mathbf{q}) \quad (23)$$

with

$$M(\mathbf{q}) \equiv m + r \sum_{k=1}^3 (1 - \cos q_k) \quad (24)$$

$$\mathbf{Q}_{\mathbf{k}}(\mathbf{q}) \equiv \sin q_k \quad (25)$$

Observing Eq.(23) and Eq.(13), we realize that a meaningful comparison requires expressing the Dirac-Wilson Hamiltonian of Eq.(22) in a representation in which the kinetic energy acquires the form of the kinetic energy piece of Eq.(13). In the continuum this representation exists and is given by the well known free Foldy-Wouthuysen (FW) transformation [11]. By this we mean a transformation where the Dirac field is rotated by the unitary transformation which decouples upper and lower components in the *absence* of interactions. Of course, the full Foldy-Wouthuysen transformation performs this decoupling including the interaction with the external field order by order in the inverse quark mass. However, we wish to avoid a large mass expansion for light quarks, and an “all-orders” version of the FW transformation is not known explicitly. Nevertheless, the relation between models  $H_2$  and  $H_3$  can still be clarified by a partial FW transformation in which upper and lower components are decoupled in the kinetic term only. On the lattice the corresponding representation goes along the same lines as in the continuum. We then write

$$H'_3 = \tilde{\chi}^+ e^{-iS} e^{iS} \mathcal{H}_3 e^{-iS} e^{iS} \tilde{\chi} \quad (26)$$

where  $e^{iS}$  is a unitary (but nonlocal) operator. In momentum space, if we choose  $e^{iS}$  according to (See [4])

$$\langle \mathbf{p} | e^{iS} | \mathbf{q} \rangle = L^3 \delta_{\mathbf{p}, \mathbf{q}} \left[ \cos \Theta_{\mathbf{q}} + \frac{\gamma^i \mathbf{Q}_i(\mathbf{q})}{|\mathbf{Q}(\mathbf{q})|} \sin \Theta_{\mathbf{q}} \right] \quad (27)$$

where  $\mathbf{Q}_i(\mathbf{q})$  is given by Eq.(25),  $\gamma^i$  are the Dirac gamma matrices, and

$$\cos \Theta_{\mathbf{q}} \equiv \frac{1}{\sqrt{2}} \sqrt{1 + \frac{1}{\sqrt{1 + \frac{|\mathbf{Q}(\mathbf{q})|^2}{M^2(\mathbf{q})}}}}} \quad (28)$$

$$\sin \Theta_{\mathbf{q}} \equiv \frac{1}{\sqrt{2}} \sqrt{1 - \frac{1}{\sqrt{1 + \frac{|\mathbf{Q}(\mathbf{q})|^2}{M^2(\mathbf{q})}}}}} \quad (29)$$

After this transformation, the kinetic part of  $H_3$  becomes

$$H'_{3 \text{ kin}} = \frac{1}{L^3} \sum_{\mathbf{p}} \Psi^\dagger(\mathbf{p}) \beta E_{\mathbf{p}} \Psi(\mathbf{p}) \quad (30)$$

where  $E_{\mathbf{p}} = \sqrt{M^2(\mathbf{p}) + \sum_{k=1}^3 \mathbf{Q}_k^2(\mathbf{q})}$ , with  $M(\mathbf{p})$  and  $\mathbf{Q}_k(\mathbf{q})$  given by (24) and (25), and  $\Psi \equiv e^{iS} \chi$ . In Ref [12], a lattice Foldy-Wouthuysen transformation is also being considered.

So now, both models have the same kinetic part and the difference between them becomes completely transparent. Namely, while the model of Eq.(13) has (in coordinate space) a potential energy of the form:

$$H_{2 \text{ pot}} = \sum_{\vec{x}} \Psi^\dagger(\vec{x}) V(\vec{x}) \Psi(\vec{x}) \quad (31)$$

the potential energy of the model  $H_3$  becomes after the Foldy-Wouthuysen transformation of Eqs (26-29):

$$\begin{aligned}
H'_{3 \text{ pot}} &= \frac{1}{L^6} \sum_{\vec{z}} \Psi^+(\vec{z}) \left\{ \sum_{\vec{x}, \vec{y}} \sum_{\vec{p}, \vec{q}} e^{i\vec{q}(\vec{z}-\vec{x})} e^{i\vec{p}(\vec{x}-\vec{y})} V(\vec{x}) \right. \\
&\quad \left. [\cos \Theta_{\mathbf{q}} + \frac{\vec{\gamma} \cdot \vec{Q}}{|\vec{Q}|} \sin \Theta_{\mathbf{q}}] [\cos \Theta_{\mathbf{p}} - \frac{\vec{\gamma} \cdot \vec{P}}{|\vec{P}|} \sin \Theta_{\mathbf{p}}] \right\} \Psi(\vec{y}) \quad (32)
\end{aligned}$$

as can be seen simply by expressing the fields  $\chi$  and  $\chi^+$  in terms of  $\Psi$  and  $\Psi^+$  through  $\chi = e^{-iS} \Psi$  and  $\chi^+ = \Psi^+ e^{iS}$ .

Comparing Eqs (31) and (32) and taking into account the definitions of  $\cos \Theta_{\mathbf{p}}$  and  $\sin \Theta_{\mathbf{p}}$  given by Eqs (28) and (29), we see that (32) reduces to (31) in the  $m \rightarrow \infty$  limit, in which  $\cos \Theta_{\mathbf{p}} \rightarrow 1$  and  $\sin \Theta_{\mathbf{p}} \rightarrow 0$  and therefore

$$\begin{aligned}
H'_{3 \text{ pot}} &\xrightarrow{m \rightarrow \infty} \frac{1}{L^6} \sum_{\vec{z}} \Psi^+(\vec{z}) \left\{ \sum_{\vec{x}, \vec{y}} \sum_{\vec{p}, \vec{q}} e^{i\vec{q}(\vec{z}-\vec{x})} e^{i\vec{p}(\vec{x}-\vec{y})} V(\vec{x}) \right\} \Psi(\vec{y}) \\
&= \sum_{\vec{x}} \Psi^+(\vec{x}) V(\vec{x}) \Psi(\vec{x}) \quad (33)
\end{aligned}$$

It is worth looking at the above limit in more detail. Expanding the product between brackets in Eq(32) and remembering that  $\gamma^i \gamma^j = g^{ij} - i\sigma^{ij}$ , we obtain

$$\begin{aligned}
H'_{3 \text{ pot}} &= \frac{1}{L^6} \sum_{\vec{z}} \Psi^+(\vec{z}) \left\{ \sum_{\vec{x}, \vec{y}} \sum_{\vec{p}, \vec{q}} e^{i\vec{q}(\vec{z}-\vec{x})} e^{i\vec{p}(\vec{x}-\vec{y})} V(\vec{x}) \right. \\
&\quad \left. [F_1(\vec{p}, \vec{q}) + F_2(\vec{p}, \vec{q}) + F_3(\vec{p}, \vec{q})] \right\} \Psi(\vec{y}) \quad (34)
\end{aligned}$$

where

$$F_1(\vec{p}, \vec{q}) = \cos \Theta_{\mathbf{q}} \cos \Theta_{\mathbf{p}} + \frac{\mathbf{Q}(\mathbf{q}) \cdot \mathbf{P}(\mathbf{p})}{|\mathbf{Q}(\mathbf{q})| |\mathbf{P}(\mathbf{p})|} \sin \Theta_{\mathbf{q}} \sin \Theta_{\mathbf{p}} \quad (35)$$

$$F_2(\vec{p}, \vec{q}) = i\sigma^{ij} \frac{\mathbf{Q}_i(\mathbf{q}) \mathbf{P}_j(\mathbf{p})}{|\mathbf{Q}(\mathbf{q})| |\mathbf{P}(\mathbf{p})|} \sin \Theta_{\mathbf{q}} \sin \Theta_{\mathbf{p}} \quad (36)$$

$$F_3(\vec{p}, \vec{q}) = \gamma^i \frac{\mathbf{Q}_i(\mathbf{q})}{|\mathbf{Q}(\mathbf{q})|} \sin \Theta_{\mathbf{q}} \cos \Theta_{\mathbf{p}} - \gamma^i \frac{\mathbf{P}_i(\mathbf{p})}{|\mathbf{P}(\mathbf{p})|} \sin \Theta_{\mathbf{p}} \cos \Theta_{\mathbf{q}} \quad (37)$$

To interpret these terms it is convenient to consider their continuum limit. In this limit, Eq(28) and (29) become:

$$\cos \Theta_{\mathbf{q}} \equiv \frac{1}{\sqrt{2}} \sqrt{1 + \frac{1}{\sqrt{1 + \frac{|\mathbf{q}|^2}{m^2}}}} \xrightarrow{m \rightarrow \text{large}} 1 - \frac{1}{8} \frac{|\mathbf{q}|^2}{m^2} \quad (38)$$

$$\sin \Theta_{\mathbf{q}} \equiv \frac{1}{\sqrt{2}} \sqrt{1 - \frac{1}{\sqrt{1 + \frac{|\mathbf{q}|^2}{m^2}}}} \xrightarrow{m \rightarrow \text{large}} \frac{1}{2} \frac{|\mathbf{q}|}{m} \quad (39)$$

and the interactions corresponding to the three terms above become:

$$H'_{3 \text{ pot}}{}^{F_1} = \int_{\vec{z}} \Psi^+(\vec{z}) \left\{ \int_{\vec{x}, \vec{y}} \int_{\vec{p}, \vec{q}} e^{i\vec{q}(\vec{z}-\vec{x})} e^{i\vec{p}(\vec{x}-\vec{y})} V(\vec{x}) \right. \\ \left. \left[ 1 - \frac{1}{8} \frac{|\mathbf{q}|^2}{m^2} - \frac{1}{8} \frac{|\mathbf{p}|^2}{m^2} + \frac{1}{4} \frac{\mathbf{q} \cdot \mathbf{p}}{m^2} \right] \right\} \Psi(\vec{y}) \quad (40)$$

$$= \int_{\vec{x}} \Psi^+(\vec{x}) V(\vec{x}) \Psi(\vec{x}) \quad (41)$$

$$+ \frac{1}{8m^2} \int_{\vec{x}} \Psi^+(\vec{x}) \nabla^2 V(\vec{x}) \Psi(\vec{x}) \quad (42)$$

Term (41) represents the electrostatic energy of a point-like particle and is the one present in models  $H_1$  and  $H_2$ . More interestingly, term (42) corresponds to exactly the Darwin term. It arises because of Zitterbewegung, as can be seen from the smearing of the potential (see Eqs(34) and (35) ).

$$H'_{3 \text{ pot}}{}^{F_2} = \int_{\vec{z}} \Psi^+(\vec{z}) \left\{ \int_{\vec{x}, \vec{y}} \int_{\vec{p}, \vec{q}} e^{i\vec{q}(\vec{z}-\vec{x})} e^{i\vec{p}(\vec{x}-\vec{y})} V(\vec{x}) \right. \\ \left. \left[ i\sigma^{ij} \frac{\mathbf{q}_i \mathbf{p}_j}{|\mathbf{q}| |\mathbf{p}|} \frac{1}{4} \frac{|\mathbf{q}| |\mathbf{p}|}{m^2} \right] \right\} \Psi(\vec{y}) \quad (43)$$

$$= \int_{\vec{z}} \Psi^+(\vec{z}) \left\{ \int_{\vec{x}, \vec{y}} \int_{\vec{p}, \vec{q}} e^{i\vec{q}(\vec{z}-\vec{x})} e^{i\vec{p}(\vec{x}-\vec{y})} V(\vec{x}) \right. \\ \left. \left[ i\epsilon_{ijk} \begin{pmatrix} \sigma^k & 0 \\ 0 & \sigma^k \end{pmatrix} \frac{\mathbf{q}_i \mathbf{p}_j}{4m^2} \right] \right\} \Psi(\vec{y}) \quad (44)$$

$$= -\frac{i}{4m^2} \int_{\vec{x}} \Psi^+(\vec{x}) \epsilon_{ijk} \frac{\partial}{\partial x_i} \left\{ V(\vec{x}) \begin{pmatrix} \sigma^k & 0 \\ 0 & \sigma^k \end{pmatrix} \frac{\partial}{\partial x_j} \Psi(\vec{x}) \right\} \quad (45)$$



Where we have used the identity  $\sigma^{ij} = \epsilon_{ijk} \begin{pmatrix} \sigma^k & 0 \\ 0 & \sigma^k \end{pmatrix}$ , where the  $\sigma^k$  are the Pauli matrices. Clearly Eq(45) represents the spin-orbit interaction.

Finally we have:

$$H'_3{}_{\text{pot}} = \int_{\vec{z}} \Psi^+(\vec{z}) \left\{ \int_{\vec{x}, \vec{y}} \int_{\vec{p}, \vec{q}} e^{i\vec{q}(\vec{z}-\vec{x})} e^{i\vec{p}(\vec{x}-\vec{y})} V(\vec{x}) \right. \\ \left. \left[ \gamma^i \frac{\mathbf{q}_i}{2m} - \gamma^i \frac{\mathbf{p}_i}{2m} \right] \Psi(\vec{y}) \right\} \quad (46)$$

$$= \frac{i}{2m} \int_{\vec{x}} \Psi^+(\vec{x}) \left\{ \frac{\partial}{\partial x^i} V(\vec{x}) \gamma^i \right\} \Psi(\vec{x}) \quad (47)$$

representing interactions between upper and lower components of the Dirac spinor. In a large mass expansion (the usual FW transformation) this term is removed by a unitary rotation at order  $1/m^2$ .

It is perhaps worth mentioning that ignoring this term completely (clearly valid for large masses only!) but *not making the large mass expansion* in (40, 43) and spin-averaging the resulting Hamiltonian, yields a modified potential model which we have studied and which yields wavefunctions very close to the full Dirac formalism. This approximation is not very well motivated however, as it seems to involve a rather inconsistent treatment in terms of a  $1/m$  development.

In retrospect we realize that potential model descriptions based on  $H_1$  and  $H_2$  are somewhat inconsistent since, as we have just seen, they effectively take the limit  $m \rightarrow \infty$  in the potential part while keeping a finite mass in the kinetic part (as first shown in Ref [2], the full relativistic kinetic energy is essential in reproducing the data). The reasonably good agreement between  $H_1$ ,  $H_2$  and the Monte Carlo data, together with the inconsistency pointed out above, deserves some comments. The validity of  $H_3$ , as clearly stated

in section 3, is based on the assumption that, even though the light quark moves fast enough for relativistic effects to be important, the time scales over which, the string connecting the quark to the static source responds to changes in the light quark position, are small compared with the time scales relevant for the light quark motion. This makes the interaction between the light and the static quark well described by the energy which would obtain if the light quark were held fixed. Models  $H_1$  and  $H_2$ , effectively taking the limit  $m \rightarrow \infty$  in the potential part and keeping a finite mass in the kinetic part, are simply making the further assumption that the confining potential is essentially constant over regions of size of the order of the light quark Compton wave-length. To see this implication we just have to remember that a Dirac particle does not move along a straight line with constant velocity but instead carries out an oscillatory motion (Zitterbewegung) with the speed of light (see [11, 13]) centered on a point which does move uniformly. This oscillatory motion is of the order of the Compton wavelength of the particle. As our light quark moves through the confining potential, its color charge explores then the field over a region of the order of its Compton wavelength and this explains the appearance of the Darwin term and all higher order terms familiar from the F-W transformation. However if over regions of the order of the Compton wavelength the field is slowly varying, it may be reasonable to ignore the smearing effects (formally higher order in  $1/m$ ) while maintaining the relativistic kinematics in the kinetic term. This seems to be the case in our situation in which, as can be seen from the reasonable success of models  $H_1$  and  $H_2$ , taking the  $m \rightarrow \infty$  limit in the potential part seems not to be a very bad thing to do (for example, at larger light quark masses than those studied here, the agreement between

the wavefunctions generated from  $H_2$  and  $H_3$  is closer). However were we going to do the same in the kinetic part, we would get a non-relativistic model that does a very bad job at reproducing the wave functions [2].

In any case, the most important lesson that we learn from the discussion above is that the differences that we saw in the previous section between the wave functions of model 2 and those of model 3 are, as we have just seen, the result of well known effects that arise when one combines quantum mechanics and relativity, which model 3 captures (to the extent that the Dirac equation captures them), but are ignored in models 1 and 2. These effects are to our knowledge visible for the first time in the context of quantitatively measured (in quenched lattice QCD) strong interaction wavefunctions.

## 5 Conclusions

We have presented the results for the 1S and 1P wave functions and energy differences between the 1S and 2S states of a fully relativistic lattice model of heavy-light mesons. These results were compared with Monte Carlo measurements of the corresponding quantities and with previous models. The results of the comparison validated the valence quark model as a good representation of heavy-light mesons, at least for the lattice sizes tested so far. In particular our fully relativistic model proved quantitatively as well as qualitatively superior to previous models. The quantitative improvement represented by our model arose simply by comparison with the data. The qualitative one came not only from the relative transparency of the approximations being done, clearly stated in the derivation of the model; a comparison of the physical content of the different models revealed that the

previous ones were somewhat inconsistent in their relative treatment of the potential and kinetic terms. It is precisely this comparison that allows a physical interpretation of the quantitative improvements of the fully relativistic models. As it turned out they can be thought of as due to Darwin and higher order effects (in the language of a Foldy-Wouthuysen treatment) arising from the quantum-relativistic delocalization of the light quark due to Zitterbewegung. It is remarkable that the Monte Carlo simulations of Ref [1] are now accurate enough to capture this phenomenon.

We expect to be able to extend the above results to much larger lattices. We are currently generalizing this work to treat mesons with two finite mass quarks. If the fully relativistic model continues to be as quantitatively accurate as the results obtained here suggest it may turn out to be a very useful tool in the study of the spectrum and static properties of charmonium and charmed and B-mesons.

## 6 Acknowledgement

It is a pleasure to thank here A. Duncan for invaluable discussions and contributions without which this paper could not have been done. I would also like to acknowledge the assistance of the Fermilab group (A.Duncan, E.Eichten, and H.Thacker) for making available the Monte Carlo data used in this paper. This work was supported in part by NSF Grant Phy-9322114 and by the US Dept. of Energy, Grant No. DE-FG02-91ER40685.

## References

- [1] A. Duncan, E. Eichten, J. Flynn, B. Hill, G. Hockney, and H. Thacker, Phys. Rev. **D51**,5101(1995).
- [2] A. Duncan, E. Eichten, and H. Thacker, Phys. Lett. **B303**, (1993) 109.
- [3] E. Schnapka, “Validity of Relativistic Potential Models in Confining Theories”, M.S. Thesis, Univ. of Pittsburgh, Aug. 1993.
- [4] M.G.Olsson and Sinisa Veseli, “A one parameter representation for the Isgur-Wise function”, Univ. of Wisconsin preprint MADPH-95-869 (February, 1995).
- [5] P. Cea, P. Colangelo, L. Cosmai, and Nardulli, Phys. Lett. B **206** (1988) 691.
- [6] K. Wilson, (1975), “Quarks and strings on a lattice”, in *New Phenomena in Subnuclear Physics*, ed. A. Zichichi (plenum Press, N.Y. ), part A, p.69.
- [7] I. Montvay, G. Münster, “Quantum Fields on a Lattice”, Cambridge University Press 1994.
- [8] H. Press et al, “Numerical Recipes in C”, p.83 et seq.,Cambridge University Press, 1992.
- [9] I am grateful for the assistance of the Fermilab group (A.Duncan, E.Eichten, and H.Thacker) for the MonteCarlo data used in this paper.
- [10] G. P. Lepage and P. B. Mackenzie, Phys. Rev. D **48** (1993) 2250.
- [11] L. Foldy, and S. A. Wouthuysen, Phys. Rev. **78**, (1950) 29.

- [12] A. El-Khadra, A. Kronfeld, and P. Mackenzie, “Massive Fermions in Lattice Gauge Theory”, in preparation.
- [13] P. A. M. Dirac, “The Principles of Quantum Mechanics”, fourth edition, Oxford Science Publication.